3774 *Biochemistry* **2010,** *49,* 3774–3782
DOI: 10.1021/bi100251u

BIOCHEMISTRY
including biophysical chemistry & molecular biology
Article

Comparison of Two Metal-Dependent Pyruvate Aldolases Related by Convergent Evolution: Substrate Specificity, Kinetic Mechanism, and Substrate Channeling[†]

Weijun Wang,[‡] Perrin Baker,[‡] and Stephen Y. K. Seah*

Department of Molecular and Cellular Biology, University of Guelph, Guelph, Ontario, Canada N1G 2W1.
[‡]These authors contributed equally

Received February 18, 2010; Revised Manuscript Received April 1, 2010

ABSTRACT: HpaI and BphI are two pyruvate class II aldolases found in aromatic *meta*-cleavage degradation pathways that catalyze similar reactions but are not related in sequence. Steady-state kinetic analysis of the aldol addition reactions and product inhibition assays showed that HpaI exhibits a rapid equilibrium random order mechanism while BphI exhibits a compulsory order mechanism, with pyruvate binding first. Both aldolases are able to utilize aldehyde acceptors two to five carbons in length; however, HpaI showed broader specificity and had a preference for aldehydes containing longer linear alkyl chains or C2-OH substitutions. Both enzymes were able to bind 2-keto acids larger than pyruvate, but only HpaI was able to utilize both pyruvate and 2-ketobutanoate as carbonyl donors in the aldol addition reaction. HpaI lacks stereospecific control producing racemic mixtures of 4-hydroxy-2-oxopentanoate (HOPA) from pyruvate and acetaldehyde while BphI synthesizes only (4*S*)-HOPA. BphI is also able to utilize acetaldehyde produced by the reduction of acetyl-CoA catalyzed by the associated aldehyde dehydrogenase, BphJ. This aldehyde was directly channeled from the dehydrogenase to the aldolase active sites, with an efficiency of 84%. Furthermore, the BphJ reductive deacylation reaction increased 4-fold when BphI was catalyzing the aldol addition reaction. Therefore, the BphI−BphJ enzyme complex exhibits unique bidirectionality in substrate channeling and allosteric activation.

The aerobic degradation of aromatic compounds by microorganisms is important for maintenance of the global carbon cycle and for removal of toxic industrial pollutants such as polychlorinated biphenyls (PCBs) (*1*, *2*). It is also important for cholesterol utilization and hence survival of *Mycobacterium tuberculosis* in host macrophages (*3*). In the *meta*-cleavage pathway, diverse aromatic compounds can be transformed, via a catechol intermediate, to 4-hydroxy-2-ketoacids which are subsequently cleaved across the C3−C4 bond by pyruvate aldolases to form pyruvate and an aldehyde (*4*, *5*). For example, BphI (EC 4.1.3.39), the aldolase in the PCBs degradation pathway of *Burkholderia xenovorans* LB400, catalyzes the aldol cleavage of 4-hydroxy-2-oxopentanoate to pyruvate and acetaldehyde (Figure 1A) (*6*). HpaI (EC 4.1.2.-) (also known as HpcH), in the 3- and 4-hydroxyphenylacetate catabolic pathway of *Escherichia coli* strain W or C, transforms 4-hydroxy-2-oxo-1,7-heptanedioate to pyruvate and succinic semialdehyde (Figure 1B) (*7*). HpaI is also able to catalyze the aldol cleavage of 4-hydroxy-2-oxopentanoate, the physiological substrate of BphI (*8*, *9*). Both HpaI and BphI share a similar reaction mechanism as they are competitively inhibited by oxalate and exhibit secondary oxaloacetate decarboxylase activity. This can be rationalized by the formation of a pyruvate enolate intermediate in their catalytic mechanisms (*10*). This pyruvate enolate intermediate is stabilized by divalent metal ions in the two enzymes reminiscent of class II aldolases (*11*, *12*) and is distinct from class I aldolases that utilize a Schiff base mechanism (*13*−*15*).

Interestingly, HpaI and BphI do not share any sequence similarities. HpaI belongs to the pyruvate/phosphoenolpyruvate family of enzymes (*16*, *17*), whose members also include citrate lyase and pyruvate kinase (*18*), while BphI belongs to the HMGL-like family of enzymes that includes its homologue DmpG from the phenol degradation pathway and the enzymes 3-hydroxy-3-methylglutaryl-CoA lyase, 2-isopropylmalate synthase, and transcarboxylase 5S (*19*). Homologues of HpaI and BphI are clustered into two different COG groups (COG3836 for HpaI and COG0119 for BphI) and are widely distributed in microorganisms (*20*, *21*). Although both the HpaI and BphI families of aldolases adopt TIM barrel folds, the HpaI hexamer is composed of $(\alpha\beta)_8$ barrels in which α_8 from each subunit forms a domain-swapped dimer with the adjacent subunit (*22*). In contrast, the BphI family of aldolases is composed of two symmetrical half-barrels, $(\alpha\beta)_{1-4}$ and $(\alpha\beta)_{5-8}$, with helical insertions between $\beta_1-\alpha_1$ and $\beta_5-\alpha_5$. They also contain an additional α-helical domain located at the C-terminus of the TIM barrel called the communication domain which plays an important role in heterodimerization with an associated acetaldehyde dehydrogenase (EC 4.1.2.10) that converts the acetaldehyde formed from the aldolase reaction to acetyl-CoA using NAD^+ and coenzyme A as cofactors (*6*, *23*). This association enables the direct channeling of the acetaldehyde product from the aldolase to the dehydrogenase, as demonstrated recently in the BphI aldolase−BphJ dehydrogenase complex. In addition, the amino acid ligands of the metal cofactor differ in HpaI and BphI (Glu^{149} and Asp^{175} in HpaI; His^{199}, His^{201}, and Asp^{18} in BphI) which may

[†]This research is supported by National Science and Engineering Research Council of Canada (NSERC) Grant 238284 (to S.Y.K.S.). P.B. is a recipient of a NSERC PGS-D scholarship.

*Corresponding author. E-mail: sseah@uoguelph.ca. Phone: (519) 824 4120 ext 56750. Fax: (519) 837 1802.

 Published on Web 04/05/2010

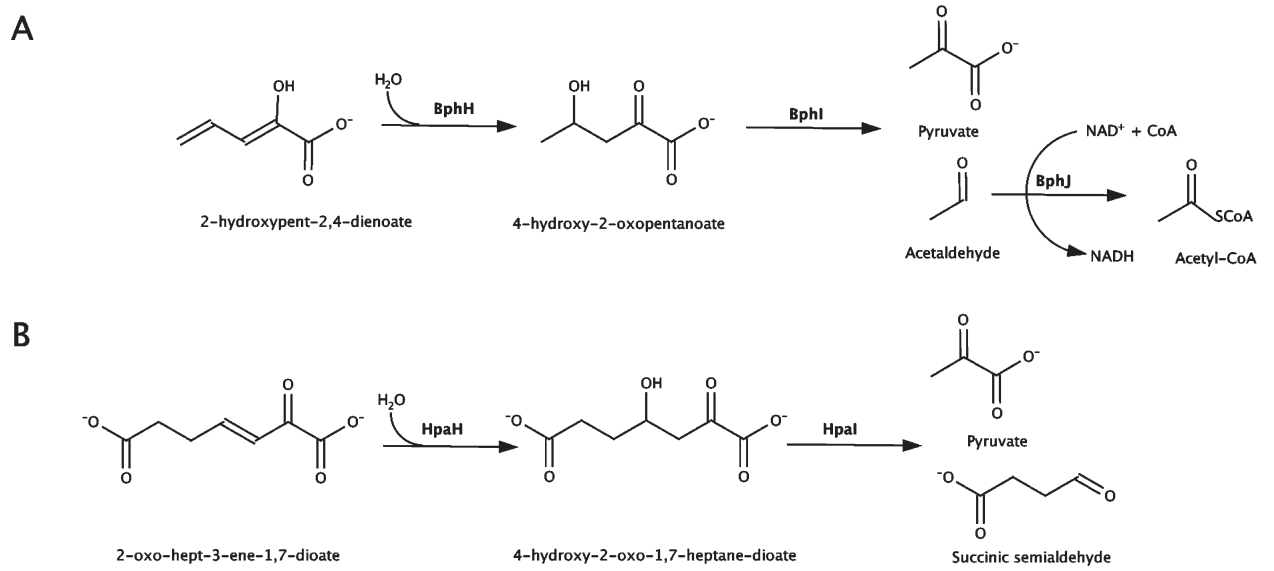

FIGURE 1: Comparison of the last steps of (A) biphenyl degradation and (B) 4-hydroxyphenylacetate and pathways. The hydratases HpaH and BphH share 35% sequence identity. However, HpaI and BphI do not share any sequence similarities. The biphenyl degradation contains one additional enzyme, an acetaldehyde dehydrogenase, BphJ.

contribute to differences in metal specificity observed in the two enzymes (*6*, *8*). Since all of TIM barrel enzymes are thought to arise from a common ancestor, the evolutionary relationship between HpaI and BphI can be best described as functional convergence after evolutionary sequence divergence.

Besides their importance in aromatic degradation pathways, pyruvate aldolases are potentially useful for synthesis of natural products and bioactive molecules due to their ability to catalyze C−C bond formation (*24*, *25*). However, compared to class I pyruvate aldolases (*13*), very little is known about class II pyruvate aldolases. Substrate specificity and kinetic analysis have only been determined in the aldol cleavage direction with a limited number of compounds (*6*, *8*). Although aldol addition assays have been reported for MhpE (80% and 56% sequence identity to BphI and DmpG, respectively), the enzyme analyzed might be a class I aldolase contaminant since it did not require metal ions for activity and was sensitive to sodium borohydride treatment (*26*). It is therefore unclear whether pyruvate class II aldolases could utilize substituted aldehydes or other 2-ketoacids besides pyruvate as substrates. The stereochemistry of the reaction catalyzed by the enzymes has also not been determined. Here, we describe a detailed comparison of the substrate specificity, stereospecificity, and kinetic mechanisms between HpaI and BphI in the aldol addition reaction. The structure−function relationship analysis of these enzymes provides an important framework, not only for future utilization and engineering of these enzymes as biocatalysts but also for modifying aromatic degradation pathways for environmental bioremediation.

EXPERIMENTAL PROCEDURES

Chemicals. Sodium pyruvate, sodium oxalate, 2-ketobutanoate, 2-ketopentanoate, 4-methyl-2-ketopentanoate, aldehydes, L-lactate dehydrogenase (LDH,[1] rabbit muscle), alcohol dehydrogenase (ADH, *Saccharomyces cerevisiae*), and Dowex 1X8−200 ion-exchange resin were from Sigma-Aldrich (Oakville, Ontario, Canada). Ni-NTA superflow resin was obtained from Qiagen (Mississauga, Ontario, Canada). HpaI and BphI-J were overexpressed and purified according to the methods previously described (*6*, *8*). All other chemicals were of analytical grade and were obtained from Sigma-Aldrich and Fisher Scientific (Nepean, Ontario, Canada).

Aldol Cleavage Activity Assay. Aldol cleavage assays were performed as previously described (*6*, *8*). To rule out the possibility that assays may be influenced by contaminating metal ions carried over from the purified enzyme, specific activities of the purified enzymes and EDTA-treated apoenzymes were determined and confirmed to be the same. For inhibition assays in the aldol cleavage reaction, concentrations of each inhibitor were varied from $0.5K_i$ to $3K_i$. Reactions were coupled with alcohol dehydrogenase (ADH) or LDH, depending on the nature of the inhibitor. Data were fitted to either a competitive or a mixed noncompetitive inhibition equation using Leonora (*27*).

Aldol Addition Activity Assay. Standard assays contained 80 mM pyruvate or 2-ketobutyric acid, 2 mM divalent metal ion, 3 μg of HpaI or 100 μg of BphI−BphJ, and aldehyde concentrations between $0.1K_m$ and to $2K_m$ in a final volume of 1.0 mL of 100 mM HEPES buffer, pH 8.0. The reaction was initiated by the addition of enzyme and proceeded for a duration of 10 min for HpaI and 120 min for BphI at 25 °C. The reaction was quenched with 200 μL of concentrated HCl and incubated overnight at 25 °C to lactonize the product. A 500 μL aliquot from each reaction was subjected to HPLC using an AKTA Explorer 100 apparatus (Amersham Pharmacia Biotech, Baie d'Urfé, Quebec, Canada) equipped with an Aminex fast-acid analysis ion-exchange column (100 mm × 7.8 mm) with a mobile phase of 0.1% formic acid at a flow rate of 0.6 mL/min. Products were detected at a wavelength of 215 nm and quantified using a standard curve of pure compounds of known concentrations. The identity of the synthesized 4-hydroxy-2-ketoacid compounds was further confirmed by ESI-qTOF MS analysis performed at the Advanced Analysis Centre, University of Guelph. Due to similar retention times for 2-dehydro-3-deoxy-L-pentonate (addition product of

[1]Abbreviations: ADH, alcohol dehydrogenase; DDG, 2-dehydro-3-deoxygalactarate; HEPES, 4-(2-hydroxyethyl)-1-piperazinepropanesulfonic acid; HOPA, 4-hydroxy-2-oxopentanoate; IPTG, isopropyl β-D-thiogalactopyranoside; LDH, L-lactate dehydrogenase; MOPS, 3-(*N*-morpholino)propanesulfonic acid; NMR, nuclear magnetic resonance.

pyruvate with glycoaldehyde) and 2-keto-3-deoxygluconate (KDG, addition product of pyruvate with glyceraldehyde), reaction rates were determined enzymatically using the HpaI cleavage reaction coupled with LDH. Following each reaction, a 500 μL aliquot of the reaction solution was filtered through a YM10 filter to remove the enzyme. Dowex 1X8−200 ion-exchange resin (sulfate form) (50 mg) was added to the flow-through and mixed for 10 min to remove pyruvate before enzymatic quantification of product formation. For substrate specificity, data were fitted to the Michaelis−Menten equation using Leonora. For kinetic mechanism assays using two varying substrates, data were fitted to a ternary complex bisubstrate equation (eq 1) using Leonora.

$$v = \frac{VAB}{K_{iA}K_{mB} + K_{mA}B + K_{mB}A + AB} \quad (1)$$

where v and V are the initial and maximal velocities, respectively, A and B are concentrations of pyruvate and acetaldehyde, K_{mA} and K_{mB} are Michaelis constants of substrates pyruvate and acetaldehyde, and K_{iA} is the dissociation constant for pyruvate (*28*).

Determination of Stereospecificity. The 4-hydroxy-2-oxoacids were synthesized by HpaI (2.5 mg) and BphI (20 mg), respectively, using 0.3 M pyruvate and 1.8 M of acetaldehyde or 0.3 mM succinic semialdehyde and 10 mM pyruvate in 10 mL of 0.1 M HEPES buffer (pH 8.0) containing 2 mM $MnCl_2$. Following incubation for 60 min, 0.5 g of Chelex 100 was added to remove all metal ions and to stop the enzyme reaction. The reaction mixture was then filtered through a YM10 filter to remove the enzyme and then separated in a Dowex 1X8−200 ion-exchange resin using a linear 0−0.1 M H_2SO_4 gradient. Fractions containing the product were neutralized to pH ~7.0 with 5.0 M NaOH and lyophilized. (4*S*)-HOPA was also generated enzymatically from catechol using XylE, TodF, and BphH as previously described (*8*). (*R*)-HOPA was generated by treatment of racemic HOPA with 8 mg of BphI in 0.1 M HEPES buffer (pH 8.0) containing 2 mM $MnCl_2$ to remove the majority of (4*S*)-HOPA. The product was purified using Dowex 1X8−200 resin and HPLC. The concentration of each enantiomer of HOPA was determined by aldol cleavage with BphI, followed by HpaI, both in a coupled assay using LDH. Optical rotation of enantiomers was determined using an Autopol III automatic polarimeter at 25 °C. The NMR spectrum was recorded with a Bruker Avance 600 MHz at 25 °C containing a cyroprobe.

Proton Exchange of 2-Ketoacids Catalyzed by HpaI and BphI. Proton exchange reactions were performed in a 5.0 mm NMR tube with an assay solution of 600 μL containing 30 mM 2-ketoacids, 2 mM divalent metal ion, and 0.2 mg of BphI−BphJ in 20 mM deuterated MOPS buffer (pD 8.0). The chemical shift of each α-proton of 2-ketoacid is as follows: pyruvate (s, 2.38 ppm), 2-ketobutyric acid (m, 2.70−2.80 ppm), 2-ketopentanoate (m, 2.69−2.72 ppm), and 4-methyl-2-oxopentanoate (m, 2.59−2.62 ppm). Enzyme was added to initiate the reaction, and the ^{1}H NMR spectrum was recorded four times every 3 min over a period of 30 min using a Bruker Avance 600 MHz spectrometer at 25 °C using previously described methods (*6*, *8*). A solution without enzyme was measured and used as a negative control.

Reverse Substrate Channeling and Channeling Efficiency. Assays contained 1 mM acetyl-CoA or acetaldehyde, 100 mM pyruvate, 1.5 mM NADH, 2 mM $MnCl_2$, and 180 μg of BphI−BphJ in 100 mM HEPES buffer (pH 8.0) with or without 20 units of ADH, respectively. The reaction was initiated by addition of acetyl-CoA. Reactions were quenched with 1/5 (v/v) concentrated HCl at 7 and 15 min and incubated overnight, and HOPA was quantified by HPLC as described earlier. Reverse channeling was also demonstrated by measuring NADH consumption at 370 nm (extinction coefficient of 2600 M^{-1} cm^{-1}). Assays were combined as mentioned above in the presence and absence of 100 mM pyruvate, 20 units of ADH, or 10 mM EDTA. The specific activity of ADH is unaffected by the small amounts of EDTA added. The productive channeling efficiency (CE) was defined as the ratio of V_3 to V_1, which can be determined by the equation:

$$\text{CE}\ (\%) = \frac{V_3}{V_1} \times 100 = \frac{V_1 - V_2}{V_1} \times 100$$
$$= \left(2 - \frac{V_1 + V_2}{V_1}\right) \times 100 = (2 - R) \times 100 \quad (2)$$

where V_1 is the rate of conversion of acetyl-CoA to acetaldehyde by BphJ, V_2 is the rate of conversion of acetaldehyde to ethanol in the bulk solvent by ADH, V_3 is the rate of aldol addition of pyruvate with acetaldehyde which is channeled from BphJ, R is the ratio of NADH oxidation with ADH compared to no ADH which is $(V_1 + V_2)/V_1$ (Figure 2).

Active Site Architecture Analysis. The structure of HpaI was analyzed using coordinates from the PDB (2V5K). The model of BphI, residues 4−340, was generated by ModWeb (*29*), an online server based on MODELLER (*30*, *31*), using the crystal structure of the homologous aldolase DmpG (1NVM:A) which has 56% sequence identity and 70% sequence similarity to BphI (*23*). A total of 117 models were generated, and the top predicted protein structure was selected and validated based on sequence identity, discrete optimized protein energy (DOPE), ModPipe protein quality score (MPQS), and MetaMQAPII (*32*). The final model had a z-DOPE of −1.27 and a MPQS of 1.65999 which is >1.1. MetaMQAPII showed that the generated model has an rmsd of 1.472 Å and GDT-TS (global distance test total score), which is a CASP measure of model quality, of 82.493. All images were generated using PyMOL (*33*).

RESULTS

Carbonyl Donor and Aldehyde Acceptor Specificity. HpaI and BphI were tested for their ability to catalyze the enolization of pyruvate analogues by monitoring the α-proton exchange rate of these compounds in deuterated buffer by ^{1}H NMR. Interestingly, HpaI was able to catalyze the proton exchange of 2-ketobutanoic acid, which is one carbon longer than the physiological carbonyl donor, pyruvate, although the $k_{exchange}$ is 60-fold lower ($k_{exchange}$ of 12.7 ± 0.3 μmol·min^{-1}·mg^{-1} versus 769 ± 22 μmol·min^{-1}·mg^{-1}). BphI was only able to catalyze the proton exchange of pyruvate with a $k_{exchange}$ of 0.32 ± 0.02 μmol·min^{-1}·mg^{-1}. Neither enzyme was able to catalyze proton exchange of 2-ketopentanoic acid and 4-methyl-2-ketopentanoic acid. To determine whether the aldolases can bind these pyruvate analogues, steady-state kinetic inhibition assays were performed. All 2-ketoacids tested were able to competitively inhibit the aldol cleavage of 4-hydroxy-2-oxopentanoate by HpaI and BphI, demonstrating that active sites of both enzymes are able to accommodate 2-ketoacids larger than pyruvate (Table 1). The inhibition constants (K_{ic}), however, increase with increasing size of the 3-subsutituent.

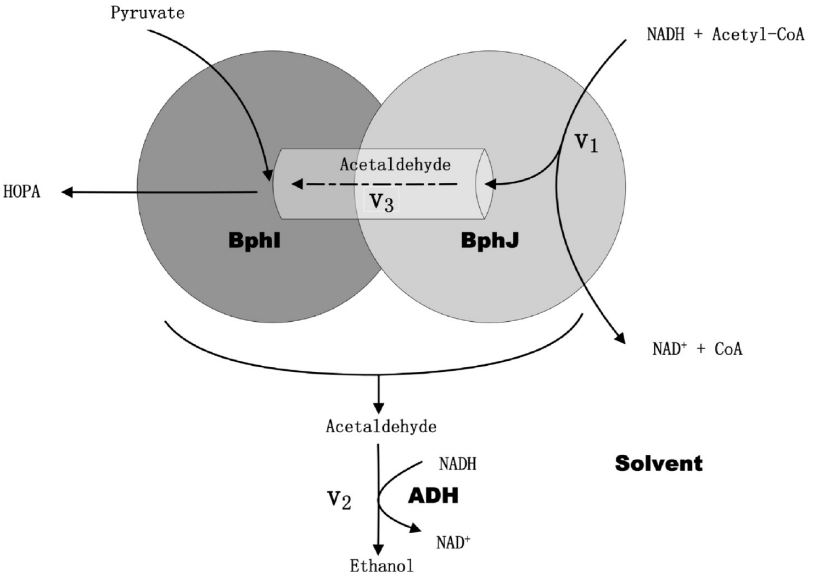

FIGURE 2: Overview of reverse channeling assay in the aldolase−dehydrogenase complex BphI−BphJ. V_1 is the rate of conversion of acetyl-CoA to acetaldehyde by BphJ, V_2 is the rate of conversion of acetaldehyde to ethanol in the bulk solvent by ADH, and V_3 is the rate of aldol addition of pyruvate with acetaldehyde by BphI.

Table 1: Inhibition Constants of 2-Ketoacids in the Aldol Cleavage of HOPA[a]

	competitive inhibition constant K_i (mM)	
2-ketoacid	HpaI	BpaI
glyoxylate	0.40 ± 0.04	0.21 ± 0.01
pyruvate	0.51 ± 0.27	0.55 ± 0.03
2-ketobutanoate	0.50 ± 0.04	0.34 ± 0.04
2-ketopentanoate	3.6 ± 0.20	1.09 ± 0.10
4-methyl-2-oxopentanoate	6.98 ± 0.33	2.71 ± 0.17

[a]Assays were performed by varying the inhibitor and substrate concentrations and contained 0.4 mM NADH, 2 mM divalent metal ions (Co^{2+} for HpaI and Mn^{2+} for BphI), and 20 units of ADH in 100 mM HEPES buffer, pH 8.0 at 25 °C, in a total volume of 1 mL.

Consistent with its ability to catalyze enolate formation in pyruvate and 2-ketobutanoic acid, HpaI is able to catalyze cross-aldol addition reactions between these carbonyl donors and various aldehydes (Table 2). In particular, the enzyme is able to utilize straight chain and branched chain aldehydes ranging from two to five carbons. The highest catalytic efficiency (k_{cat}/K_m) was obtained for succinic semialdeyde, the physiological substrate of HpaI. A ~2-fold decrease in K_m and similar k_{cat} values were observed for glycoaldehyde compared to acetaldehyde, which lacks the C2-OH substituent. In comparison, an 11- and 170-fold decrease in catalytic efficiencies was observed for isobutyraldehyde and (D,L)-glyceraldehyde, which have C3-methyl and C2,C3-OH substitutions, respectively, compared to the nonsubstituted propionaldehyde. Thus, C3-OH substitution in aldehyde acceptors results in a dramatic decrease in catalytic efficiency. Using 2-ketobutanoic acid as a carbonyl donor and acetaldehyde as acceptor, HpaI showed a 10-fold decrease in catalytic efficiency relative to pyruvate. This decrease is the result of a lower k_{cat} value, as K_m differed by less than 2-fold.

BphI, on the other hand, can only utilize pyruvate as a carbonyl donor and preferentially utilizes straight chain aldehydes as carbonyl acceptors. The enzyme has the highest specificity constants (k_{cat}/K_m) for aldehydes of two to three carbons in length. The similar specificity constants (k_{cat}/K_m) obtained for acetaldehyde and propionaldehyde are consistent with the similar specificity of the enzyme toward the corresponding 4-hydroxy-2-oxopentanoate and 4-hydroxy-2-oxohexanoate substrates in the aldol cleavage direction (*6*). Longer chain aldehydes resulted in dramatic decrease in catalytic efficiencies, due to the high K_m values for these substrates. Unlike HpaI, aldehydes substituted with C2- and C3-OH are not substrates of BphI.

Stereospecificity Control. Besides their distinct substrate specificity, HpaI and BphI differ in the stereospecific control of the aldol addition and cleavage reactions. HOPA synthesized using Mn^{2+}-HpaI or Mn^{2+}-BphI have identical structures as determined by ^1H and ^{13}C NMR but differ in optical rotation (Table S2). The optical rotation of HOPA produced by BphI is similar to the (4*S*)-HOPA produced from catechol using catechol dioxygenase (XylE), 2-hydroxy-6-oxo-2,4-heptadienoate hydrolase (TodF), and 2-hydroxypenta-2,4-dienoate hydratase (BphH) ($[\alpha]^{25}_D$ = 15.4 and 12.3, respectively) (*34*), indicating that the aldol addition reaction catalyzed by BphI only produces (4*S*)-HOPA. On the other hand, the optical rotation of HOPA synthesized by HpaI is 0.11, indicative of a racemic mixture of (4*R*)- and (4*S*)-HOPA in approximately equal concentrations. In addition, BphI was only able to cleave approximately 53% of the HOPA synthesized by HpaI, leaving a HOPA product (*R*-isomer) with an optical rotation of −11.3. On the other hand, HpaI was able to cleave both (4*R*)- and (4*S*)-HOPA. The 4-hydroxy-2-oxo-1,7-heptanedioate, synthesized by HpaI, had an optical rotation of 0.05, which indicates that the enzyme is also not stereospecific for its physiological substrate.

Determination of Kinetic Mechanism of the Aldol Addition Reaction. Kinetic assays were performed using varying concentrations of pyruvate and acetaldehyde in the aldol addition reaction. Lineweaver−Burk plots of the results show a series of converging lines consistent with a classical ternary complex bi-uni mechanism in both HpaI and BphI (Figure S2) (*35*). The k_{cat} of HpaI in the addition reaction is ~200 times higher than BphI (Table 3).

In order to determine the order of substrate binding in the two aldolases, product inhibition assays were further performed. Both pyruvate and acetaldehyde competitively inhibit the aldol

Table 2: Aldehyde Specificity of HpaI and BphI in the Aldol Addition Reaction[a]

carbon length		structure	HpaI $K_{m,app}$ (mM)	HpaI $k_{cat,app}$ (s^{-1})	HpaI $(k_{cat}/K_m)_{app}$ ($\times 10^3$ M^{-1} s^{-1})	BphI $K_{m,app}$ (mM)	BphI $k_{cat,app}$ (s^{-1})	BphI $(k_{cat}/K_m)_{app}$ (M^{-1} s^{-1})
	pyruvate as carbonyl donor							
2	acetaldehyde	CH_3CHO	62.9 ± 4.7	205.4 ± 5.2	3.3 ± 0.3	64.28 ± 3.72	0.86 ± 0.02	13.4 ± 0.80
	glycolaldehyde	$CH_2(OH)CHO$	33.3 ± 6.1	175.5 ± 8.8	5.27 ± 0.3	124.6 ± 9.6	0.40 ± 0.01	3.7 ± 0.31
3	propionaldehyde	CH_3CH_2CHO	32.9 ± 0.9	358.4 ± 3.5	10.9 ± 0.3	135.9 ± 9.6	1.79 ± 0.07	13.2 ± 1.1
	(D,L)-glyceraldehyde	$CH_2(OH)CH(OH)CHO$	88.6 ± 12.0	5.6 ± 0.42	0.063 ± 0.005	ND	ND	ND
4	butyraldehyde	$CH_3(CH_2)_2CHO$	13.4 ± 1.5	132.5 ± 4.6	9.9 ± 1.2			2.19 ± 0.12[b]
	isobutyraldehyde	$(CH_3)_2CHCHO$	73.8 ± 6.2	64.9 ± 2.7	0.9 ± 0.1			0.50 ± 0.04[b]
	succinic semialdehyde	$COOH(CH_2)_2CHO$	9.1 ± 0.9	203.8 ± 7.7	22.5 ± 2.3	ND	ND	ND
5	pentaldehyde	$CH_3(CH_2)_3CHO$			20.0 ± 0.3[b]			0.47 ± 0.01[b]
	2-ketobutanoate as carbonyl donor							
2	acetaldehyde	CH_3CHO	50.1 ± 4.3	21.9 ± 0.6	0.4 ± 0.04	ND	ND	ND

[a]Assays were performed at 25 °C and contained 7.7 μg of HpaI or 120 μg of BphI, 2 mM $CoCl_2$ for HpaI and 2 mM $MnCl_2$ for BphI, and 100 mM pyruvate with varying concentrations of aldehydes. Reactions were 10 min in duration for HpaI and 120 min in duration for BphI. 4-Hyroxy-2-ketoacids formed were lactonized and detected at 215 nm by HPLC analysis using an Aminex fast-acid analysis ion-exchange column. ND denotes no detectable activity. [b]Due to low substrate solubility and the high apparent K_m for this substrate, the specificity constant can be estimated from only the gradient of the specific activity vs substrate concentration graph. All synthesized products were confirmed using HPLC and ESI-qTOF-MS (Table S1).

Table 3: Steady-State Kinetic Parameters of HpaI and BphI for the Aldol Addition Reaction[a]

enzyme	k_{cat} (s^{-1})	K_{iA} (mM)	K_{mA} (mM)	K_{mB} (mM)
HpaI	219.5 ± 5.9	2.01 ± 0.40	5.6 ± 0.5	62.1 ± 4.0
BphI	1.04 ± 0.05	10.3 ± 0.10	14.8 ± 1.4	67.0 ± 6.3

[a]Assays were performed at 25 °C and contained 7.7 μg of HpaI or 120 μg of BphI, 2 mM $CoCl_2$ for HpaI and 2 mM $MnCl_2$ for BphI, and varying concentrations of pyruvate (substrate A) and acetaldehyde (substrate B). Reactions were 10 min in duration for HpaI and 120 min in duration for BphI. Kinetic parameters were determined using a discontinuous assay method as described in Experimental Procedures.

Table 4: HOPA Formation during an ADH Competition Assay[a]

[substrate]	reaction time (min)	HOPA concn (μM) without ADH	HOPA concn (μM) with ADH
acetyl-CoA	7	175.4 ± 2.6	140.8 ± 0.01
	15	198.1 ± 1.0	160.6 ± 5.6
acetaldehyde	7	13.0 ± 1.5	ND
	15	25.9 ± 0.5	ND

[a]Assays were performed at 25 °C and contained 1 mM acetyl-CoA, 100 mM pyruvate, 1.5 mM NADH, and 2 mM $MnCl_2$ in the presence and absence of 20 units of ADH in 100 mM HEPES buffer (pH 8.0) in a total volume of 1 mL. Lactonized HOPA was detected and quantified using absorbance at 215 nm. ND denotes no detectable product.

cleavage of HOPA by HpaI, indicating that either compound is able to bind to the free enzyme (Figure S3). Therefore, HpaI follows a rapid equilibrium random order mechanism. On the other hand, BphI exhibits competitive inhibition for pyruvate but mixed inhibition for acetaldehyde, indicating that the enzyme obeys a compulsory or preferred order mechanism in the aldol addition reaction with pyruvate binding to the active site prior to acetaldehyde. Similar results were obtained using Mn^{2+}-HpaI, confirming that the distinct kinetic mechanisms between HpaI and BphI are not due to the differences in metal cofactor used in the assays.

Reverse Substrate Channeling in the BphI−BphJ Complex. BphI forms a complex with the acetaldehyde dehydrogenase, BphJ, permitting their active sites to be linked by a molecular tunnel. We previously demonstrated that acetaldehyde, produced from aldol cleavage of HOPA, can be directly channeled from the aldolase to the dehydrogenase, where it is then converted to acetyl-CoA in the presence of NAD^+ and coenzyme A (*6*). Since BphJ can catalyze the reverse reaction, transforming acetyl-CoA to acetaldehyde, we investigated if aldehyde channeling can occur in reverse, and whether this would increase the efficiency of HOPA synthesized by BphI. Reverse substrate channeling was assessed by including alcohol dehydrogenase (ADH) in the assay mixture, which would convert any acetaldehyde that is released to the bulk solvent to ethanol. Table 4 shows a summary of the results obtained from HPLC analyses of reaction products. Control reactions using acetaldehyde in place of acetyl-CoA showed that ADH effectively competes with BphI for exogenous acetaldehyde since no HOPA can be detected. When acetyl-CoA is used in place of acetaldehyde, HOPA was synthesized, and addition of ADH in the reaction resulted in only a ~20% reduction of HOPA produced, suggesting that the majority of acetaldehyde formed during the BphJ reductive deacylation reaction is not released into the bulk solvent but is channeled directly to BphI (~80% channeling efficiency). Furthermore, a 16-fold greater concentration of HOPA is formed using acetyl-CoA than an equivalent amount of acetaldehyde added exogenously without ADH in the reaction mixture. The high K_m for acetaldehyde in BphI appears to be compensated by the direct channeling of acetaldehyde from BphJ, allowing BphI to experience a higher concentration of this substrate.

Using NADH oxidation assay it is also possible to confirm and quantify the reverse channeling efficiency (Figure 2). In the absence of pyruvate, NADH oxidation rate by BphJ during the conversion of acetyl-CoA to acetaldehyde is 3.85×10^{-2} $\mu mol \cdot min^{-1} \cdot mg^{-1}$, and this rate increased 2-fold following addition of ADH, as ADH will also oxidize NADH when transforming the acetaldehyde released by BphJ into ethanol

(Table 5). However, when pyruvate is present in the same assay, NADH oxidation rates only differ by 1.l6-fold, whether ADH was present or not, providing evidence that acetaldehyde is channeled from BphJ to BphI to form HOPA and is unavailable for oxidation by ADH. Upon addition of EDTA, which chelates the Mn^{2+} cofactor and inactivates BphI, a 2-fold increase in NADH oxidation is again observed upon addition of ADH. From these results and eq 2, channeling efficiency was determined to be 84%, which is in agreement with our earlier estimate from analysis of amounts of HOPA produced.

Table 5: Rates of NADH Oxidation in an ADH Competition Assay To Test for Substrate Channeling in the BphI−BphJ Complex[a]

	NADH oxidation activity ($\times 10^{-2}$ μmol·min^{-1}·mg^{-1})		
	0 mM pyruvate	100 mM pyruvate	100 mM pyruvate + 10 mM EDTA
no ADH	3.85 ± 0.17	16.6 ± 0.35	3.92 ± 0.13
with ADH	7.85 ± 0.12	19.2 ± 0.67	7.83 ± 0.19
ratio (R)	2.03	1.16	2.00
CE (%)	−3 (~0)	84	0

[a]Assays were performed at 25 °C and contained 1 mM acetyl-CoA, 100 mM pyruvate, 1.5 mM NADH, and 2 mM $MnCl_2$ in the presence and absence of 20 units of ADH in 100 mM HEPES buffer (pH 8.0) in a total volume of 1 mL. R is the ratio of NADH oxidation activity in the presence and absence of ADH. CE is the aldehyde channeling efficiency calculated by eq 2.

We also observed that the rate of reductive deacylation of acetyl-CoA to acetaldehyde, catalyzed by BphJ, increased ~4-fold upon addition of 100 mM pyruvate, but not the pyruvate enolate analogue, oxalate, to the BphI−BphJ complex. When BphI activity was inhibited through addition of EDTA, this allosteric activation was abolished. Thus, bound pyruvate or other intermediates in the aldol addition reaction catalyzed by BphI activates BphJ reductive deacylation activity.

Active Site Architecture Analysis. The structures of HpaI and BphI were compared using the crystal structure of HpaI from the PDB (2V5K) and a model of BphI, built by using the functionally similar homologous aldolase, DmpG, as a template (56% sequence identity) (*23*). The active site of HpaI is formed by ~30 residues from adjacent dimers and consists of an ~15 Å deep bell-shaped cleft with an ~12 Å wide mouth. This broad entrance to the active site is predominantly lined with noncharged residues and a few positively charged residues (Figure 3A).

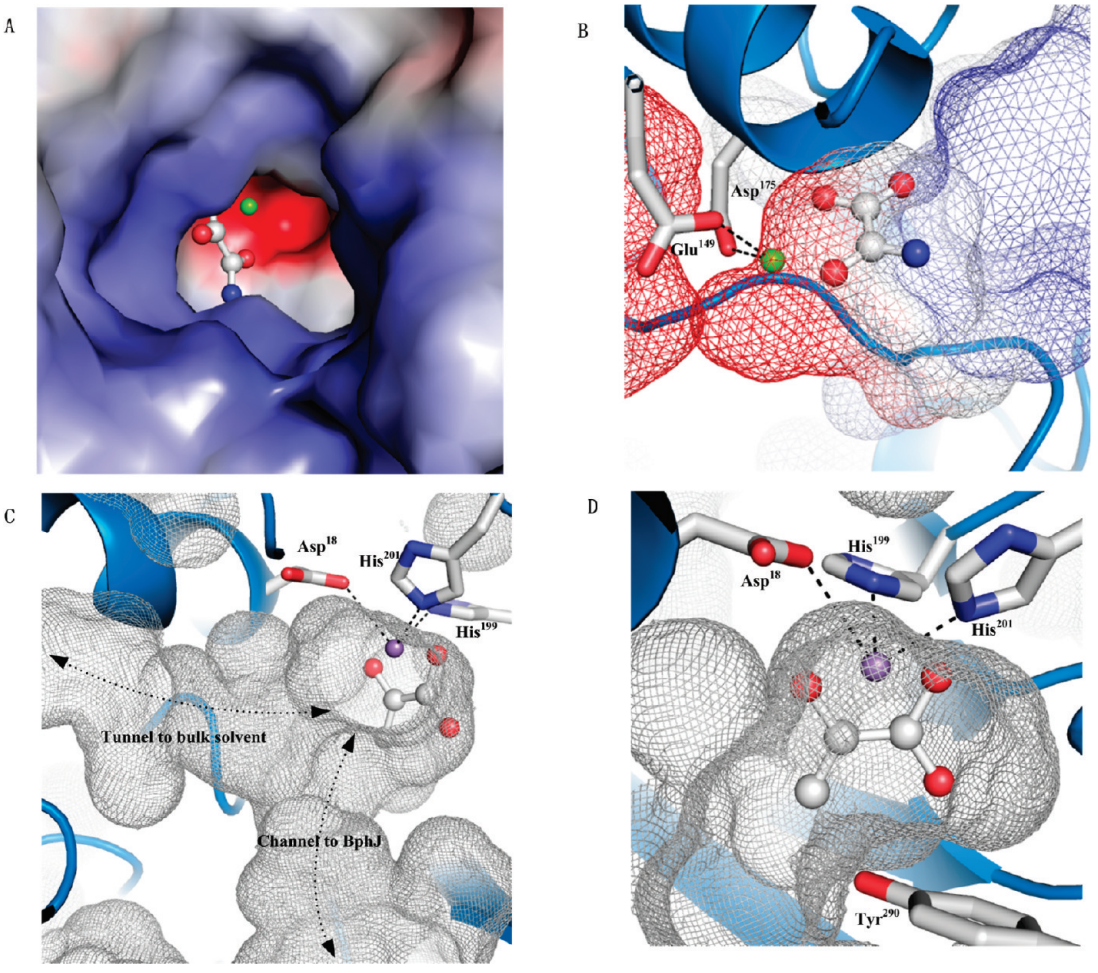

FIGURE 3: Comparison of active site architecture between HpaI and BphI. (A) Top view surface representation of the entrance to the active site of HpaI. The image is colored using generated electrostatics. Oxamate, an analogue of pyruvate enolate, is depicted in ball and stick representation. The metal ion, Mg^{2+}, is shown as a green sphere. (B) Side view of the HpaI active site cavity is depicted in mesh showing generated electrostatics. The metal ion ligands Glu^{149} and Asp^{175} are shown in sticks ligated to Mg^{2+}. (C) The active site of BphI, buried in the C terminus of the TIM barrel, has a diameter of 9.0 Å and width of 2−4 Å. Entrance to the active site occurs through two molecular tunnels shown as gray mesh. (D) The hydroxyl group of Tyr^{290} in BphI, shown in stick form, causes one side the active site to be narrowed. Based on the position of oxalate binding in DmpG, pyruvate was modeled in ball and stick representation into the innermost part of the substrate binding site. The metal ligands Asp^{18}, His^{199}, and His^{201} are shown as sticks interacting with the Mn^{2+}, shown as a purple sphere. All images were generated in PyMOL.

Oxamate, an analogue of pyruvate enolate, is coordinated to the metal ion and is positioned on one side of the cleft, an equivalent position as pyruvate in the YfaU structure (PDB 2VWT, 53% sequence identity, rmsd 0.6 Å to HpaI−Mg^{2+}-oxamate complex) (*18*). There is space distal to the pyruvate methyl carbon that can accommodate large aldehydes (Figure 3B).

The model of BphI displays a small internal active site deeply buried in the C-terminus of the TIM barrel, with a diameter of 9.0 Å and width of 2−4 Å. Noticeably, the hydroxyl group of Tyr^{290} penetrates into the active site causing the side perpendicular to the metal ligands to be narrowed. A 10 Å long narrow tunnel leads to the bulk solvent, allowing substrates to enter. A second tunnel, composed of hydrophobic residues, presumably connects to the active site of BphJ, to allow for channeling of aldehydes from the aldolase to the dehydrogenase (Figure 3C). Based on the position of oxalate binding in DmpG, pyruvate is proposed to bind to the innermost part of the substrate binding site, with the two carboxylate oxygen atoms (O1 and O3) of pyruvate forming equatorial ligands to the metal ion (Figure 3D) (*23*). This leaves a small space for aldehyde binding close to the entrance.

DISCUSSION

HpaI and BphI are class II pyruvate aldolases that catalyze similar reactions in aromatic *meta*-cleavage pathway but exhibit no sequence similarities and differ in detailed structural topology. Analysis of the two enzymes in the aldol addition reactions revealed intriguing differences in their kinetic mechanisms, stereospecificity, and substrate specificity which can be reasonably correlated to the architecture of their respective active sites.

HpaI has a wide entrance leading from the bulk solvent to the active site which may explain the rapid equilibrium random order kinetic mechanism observed in the aldol addition reaction. In contrast, the active site of BphI is smaller, with the aldehyde binding site closer to the entrance and pyruvate binding site in the interior. Therefore, pyruvate binding must precede aldehyde binding in this enzyme in order for the aldol addition to occur. Similarly, aldehyde produced in the aldol cleavage reaction must dissociate from the active site and be channeled prior to dissociation of pyruvate. The small size of the BphI active site may also cause steric constraints which allow pyruvate enolate to only attack the *re* face of acetaldehyde, thereby forming (4*S*)-HOPA (Figure S1). In contrast, the larger substrate binding site of HpaI enables the enzyme to utilize 2-ketobutyrate in place of pyruvate as the carbonyl donor and bulky aldehydes as carbonyl acceptors and permits aldehydes to bind in alternative conformations, leading to formation of racemic products. The aldol addition reaction catalyzed by 2-keto-3-deoxygluconate aldolase from *Solfolobus solfataricus* has also been reported to be non-stereospecific (*36*). Thus, the poor facial selectivity observed in HpaI is not unique among aldolases.

We have previously demonstrated that acetaldehyde and propionaldehyde, products of the BphI aldol cleavage reaction, are directly channeled to the dehydrogenase (*6*). Substrate channeling in other bifunctional complexes with a molecular tunnel, such as tryptophan synthase, has only been shown experimentally to occur in one direction (*37*). Structural analysis of the homologous aldolase−dehydrogenase complex (DmpG−DmpF) from the phenol degradation pathway has suggested that acetaldehyde channeling is finely controlled and gated by the ordered movement of Tyr^{291} (Tyr^{290} in BphI) at the entrance of the channel and the combined ordered movements of Ile^{172}, Ile^{196}, and Met^{198} (equivalent to Ile^{171}, Leu^{195}, and Met^{197} in BphJ) at the exit of the channel (*23*). Our results indicate that acetaldehyde can be efficiently channeled in the reverse direction, providing the first known example of bidirectional substrate channeling using the native substrate and demonstrating either that gating through the channel does not occur or that the proposed gating mechanism is reversible. Enzymes that exhibit substrate channeling are often allosterically regulated (*38*−*41*), ensuring that reactions occurring in separate active sites are coupled. In the reverse channeling reaction, BphI activity was demonstrated to stimulate the activity of BphJ by ∼4-fold. A similar relationship was previously observed in forward channeling where catalysis of BphJ stimulates activity of BphI ∼5-fold (*6*). This suggests that allosteric activation may be bidirectional or that the presence of pyruvate leads to the rapid conversion of acetaldehyde to HOPA resulting in faster release of products from the BphJ active site.

Aldolases homologous to HpaI are not restricted to aromatic catabolic pathways. These homologues include YfaU (*18*), involved in rhamnose degradation, and 2-dehydro-3-deoxygalactarate aldolase (*12*), involved in the galactarate degradation pathway in *E. coli*. The products of these aldolases are pyruvate and long aliphatic and hydrophilic aldehydes. The large active sites of HpaI and homologues allow them to utilize diverse substrates which may explain the recruitment of these enzymes in diverse metabolic pathway. In comparison, BphI and its homologues are mainly found in aromatic degradative pathways (*42*−*44*). The strict substrate specificity resulting from small active sites of the enzymes may limit the recruitment of these enzymes in aromatic degradation pathways, where aldol cleavage products are pyruvate and a small volatile and toxic aldehyde, such as acetaldehyde and propionaldehyde. Therefore, these aldolases are always associated with a dehydrogenase that converts toxic aldehydes to acyl-CoA. Although none of the other HMGL-like family members associate with another enzyme or exhibit substrate channeling, most of them possess an additional domain at the C-terminus of the TIM barrel domain, which can perhaps evolve to form associations with other enzymes or to regulate catalysis (*45*).

The apparent broad substrate specificity of HpaI, combined with a high turnover number, is an advantage for its use as a biocatalyst for carbon−carbon bond formation reactions in organic synthesis. However, this enzyme shows poor stereospecificity. Our results demonstrate that the use of BphI or HpaI and BphI in tandem is a promising method to produce compounds with only (*S*)- or (*R*)-conformations at C4. In addition, the reverse substrate channeling exhibited by the BphI−BphJ complex poses a unique strategy for organic synthesis, through the use of acyl-CoAs in place of aldehydes as cosubstrates to achieve higher product transformation efficiency. The comparison of kinetic mechanisms and substrate specificities will guide ongoing structural and mutagenesis studies aimed at designing pyruvate aldolases with novel substrate specificities and stereospecificities.

ACKNOWLEDGMENT

The authors thank Dan Pan for assistance in BphI−BphJ purification and Dyanne Brewer from the University of Guelph's Advanced Analysis Centre for mass spectrometry spectra acquisition.

SUPPORTING INFORMATION AVAILABLE

Facial selection of the carbonyl donor pyruvate enolate in aldol addition reaction of 4-hydroxy-2-oxopentanoate (HOPA) by HpaI and BphI (Figure S1), Lineweaver−Burk plots of HpaI and BphI in the aldol addition reaction (Figure S2), Lineweaver−Burk plots of the product inhibition of HpaI and BphI in the HOPA aldol cleavage reaction (Figure S3), HPLC and Q-Tof-MS analysis of products synthesized by aldolases (Table S1), and optical rotation and NMR analysis of HOPA produced in aldol addition reaction by HpaI and BphI (Table S2). This material is available free of charge via the Internet at http://pubs.acs.org.

REFERENCES

1. Furukawa, K., and Kimura, N. (1995) Biochemistry and genetics of PCB metabolism. *Environ. Health Perspect. 103* (Suppl. 5), 21–23.
2. Diaz, E. (2004) Bacterial degradation of aromatic pollutants: a paradigm of metabolic versatility. *Int. Microbiol. 7*, 173–180.
3. Van der Geize, R., Yam, K., Heuser, T., Wilbrink, M. H., Hara, H., Anderton, M. C., Sim, E., Dijkhuizen, L., Davies, J. E., Mohn, W. W., and Eltis, L. D. (2007) A gene cluster encoding cholesterol catabolism in a soil actinomycete provides insight into *Mycobacterium tuberculosis* survival in macrophages. *Proc. Natl. Acad. Sci. U.S.A. 104*, 1947–1952.
4. Furukawa, K., Hirose, J., Suyama, A., Zaiki, T., and Hayashida, S. (1993) Gene components responsible for discrete substrate specificity in the metabolism of biphenyl (bph operon) and toluene (tod operon). *J. Bacteriol. 175*, 5224–5232.
5. Furukawa, K., Simon, J. R., and Chakrabarty, A. M. (1983) Common induction and regulation of biphenyl, xylene/toluene, and salicylate catabolism in *Pseudomonas paucimobilis*. *J. Bacteriol. 154*, 1356–1362.
6. Baker, P., Pan, D., Carere, J., Rossi, A., Wang, W., and Seah, S. Y. (2009) Characterization of an aldolase−dehydrogenase complex that exhibits substrate channeling in the polychlorinated biphenyls degradation pathway. *Biochemistry 48*, 6551–6558.
7. Prieto, M. A., Diaz, E., and Garcia, J. L. (1996) Molecular characterization of the 4-hydroxyphenylacetate catabolic pathway of *Escherichia coli* W: engineering a mobile aromatic degradative cluster. *J. Bacteriol. 178*, 111–120.
8. Wang, W., and Seah, S. Y. (2005) Purification and biochemical characterization of a pyruvate-specific class II aldolase, HpaI. *Biochemistry 44*, 9447–9455.
9. Wang, W., and Seah, S. Y. (2008) The role of a conserved histidine residue in a pyruvate-specific class II aldolase. *FEBS Lett. 582*, 3385–3388.
10. Ash, D. E., Emig, F. A., Chowdhury, S. A., Satoh, Y., and Schramm, V. L. (1990) Mammalian and avian liver phosphoenolpyruvate carboxykinase. Alternate substrates and inhibition by analogues of oxaloacetate. *J. Biol. Chem. 265*, 7377–7384.
11. Gallo, A. A., and Sable, H. Z. (1973) Rate enhancement of pyruvate aldolization by divalent cations: a model for class II aldolases. *Biochim. Biophys. Acta 302*, 443–456.
12. Izard, T., and Blackwell, N. C. (2000) Crystal structures of the metal-dependent 2-dehydro-3-deoxy-galactarate aldolase suggest a novel reaction mechanism. *EMBO J. 19*, 3849–3856.
13. Choi, K. H., Shi, J., Hopkins, C. E., Tolan, D. R., and Allen, K. N. (2001) Snapshots of catalysis: the structure of fructose-1,6-(bis)-phosphate aldolase covalently bound to the substrate dihydroxyacetone phosphate. *Biochemistry 40*, 13868–13875.
14. Heine, A., Luz, J. G., Wong, C. H., and Wilson, I. A. (2004) Analysis of the class I aldolase binding site architecture based on the crystal structure of 2-deoxyribose-5-phosphate aldolase at 0.99Å resolution. *J. Mol. Biol. 343*, 1019–1034.
15. Morse, D. E., and Horecker, B. L. (1968) The mechanism of action of aldolases. *Adv. Enzymol. Relat. Areas Mol. Biol. 31*, 125–181.
16. Schmitzberger, F., Smith, A. G., Abell, C., and Blundell, T. L. (2003) Comparative analysis of the *Escherichia coli* ketopantoate hydroxymethyltransferase crystal structure confirms that it is a member of the (betaalpha)8 phosphoenolpyruvate/pyruvate superfamily. *J. Bacteriol. 185*, 4163–4171.
17. Narayanan, B. C., Niu, W., Han, Y., Zou, J., Mariano, P. S., Dunaway-Mariano, D., and Herzberg, O. (2008) Structure and function of PA4872 from *Pseudomonas aeruginosa*, a novel class of oxaloacetate decarboxylase from the PEP mutase/isocitrate lyase superfamily. *Biochemistry 47*, 167–182.
18. Rea, D., Hovington, R., Rakus, J. F., Gerlt, J. A., Fulop, V., Bugg, T. D., and Roper, D. I. (2008) Crystal structure and functional assignment of YfaU, a metal ion dependent class II aldolase from *Escherichia coli* K12. *Biochemistry 47*, 9955–9965.
19. Forouhar, F., Hussain, M., Farid, R., Benach, J., Abashidze, M., Edstrom, W. C., Vorobiev, S. M., Xiao, R., Acton, T. B., Fu, Z., Kim, J. J., Miziorko, H. M., Montelione, G. T., and Hunt, J. F. (2006) Crystal structures of two bacterial 3-hydroxy-3-methylglutaryl-CoA lyases suggest a common catalytic mechanism among a family of TIM barrel metalloenzymes cleaving carbon-carbon bonds. *J. Biol. Chem. 281*, 7533–7545.
20. Tatusov, R. L., Natale, D. A., Garkavtsev, I. V., Tatusova, T. A., Shankavaram, U. T., Rao, B. S., Kiryutin, B., Galperin, M. Y., Fedorova, N. D., and Koonin, E. V. (2001) The COG database: new developments in phylogenetic classification of proteins from complete genomes. *Nucleic Acids Res. 29*, 22–28.
21. Tatusov, R. L., Galperin, M. Y., Natale, D. A., and Koonin, E. V. (2000) The COG database: a tool for genome-scale analysis of protein functions and evolution. *Nucleic Acids Res. 28*, 33–36.
22. Rea, D., Fulop, V., Bugg, T. D., and Roper, D. I. (2007) Structure and mechanism of HpcH: a metal ion dependent class II aldolase from the homoprotocatechuate degradation pathway of *Escherichia coli*. *J. Mol. Biol. 373*, 866–876.
23. Manjasetty, B. A., Powlowski, J., and Vrielink, A. (2003) Crystal structure of a bifunctional aldolase-dehydrogenase: sequestering a reactive and volatile intermediate. *Proc. Natl. Acad. Sci. U.S.A. 100*, 6992–6997.
24. Takayama, S., McGarvey, G. J., and Wong, C. H. (1997) Microbial aldolases and transketolases: new biocatalytic approaches to simple and complex sugars. *Annu. Rev. Microbiol. 51*, 285–310.
25. Samland, A. K., and Sprenger, G. A. (2006) Microbial aldolases as C-C bonding enzymes—unknown treasures and new developments. *Appl. Microbiol. Biotechnol. 71*, 253–264.
26. Pollard, J. R., Rialland, D., and Bugg, T. D. (1998) Substrate selectivity and biochemical properties of 4-hydroxy-2-keto-pentanoic acid aldolase from *Escherichia coli*. *Appl. Environ. Microbiol. 64*, 4093–4094.
27. Cornish-Bowden, A. (1995) Analysis of Enzyme Kinetic Data, Oxford University Press, New York.
28. Cornish-Bowden, A. (1995) Fundamentals of Enzyme Kinetics, Portland Press, London.
29. Eswar, N., John, B., Mirkovic, N., Fiser, A., Ilyin, V. A., Pieper, U., Stuart, A. C., Marti-Renom, M. A., Madhusudhan, M. S., Yerkovich, B., and Sali, A. (2003) Tools for comparative protein structure modeling and analysis. *Nucleic Acids Res. 31*, 3375–3380.
30. Eswar, N., Webb, B., Marti-Renom, M. A., Madhusudhan, M. S., Eramian, D., Shen, M. Y., Pieper, U., Sali, A. (2006) Comparative protein structure modeling using Modeller, Current Protocols in Bioinformatics, Chapter 5, Unit 5 6.
31. Eswar, N., Eramian, D., Webb, B., Shen, M. Y., and Sali, A. (2008) Protein structure modeling with MODELLER. *Methods Mol. Biol. 426*, 145–159.
32. Pawlowski, M., Gajda, M. J., Matlak, R., and Bujnicki, J. M. (2008) MetaMQAP: a meta-server for the quality assessment of protein models. *BMC Bioinf. 9*, 403.
33. DeLano, W. L. (2002) The PyMOL Molecular Graphics System, DeLano Scientific, San Carlos, CA.
34. Collinsworth, W. L., Chapman, P. J., and Dagley, S. (1973) Stereospecific enzymes in the degradation of aromatic compounds by *Pseudomonas putida*. *J. Bacteriol. 113*, 922–931.
35. Cleland, W. W., and Cook, P. F. (2007) Enzyme Kinetics and Mechanism, Garland Science, New York, NY.
36. Lamble, H. J., Heyer, N. I., Bull, S. D., Hough, D. W., and Danson, M. J. (2003) Metabolic pathway promiscuity in the archaeon *Sulfolobus solfataricus* revealed by studies on glucose dehydrogenase and 2-keto-3-deoxygluconate aldolase. *J. Biol. Chem. 278*, 34066–34072.
37. Dunn, M. F., Aguilar, V., Brzovic, P., Drewe, W. F., Jr., Houben, K. F., Leja, C. A., and Roy, M. (1990) The tryptophan synthase bienzyme complex transfers indole between the alpha- and beta-sites via a 25−30 Å long tunnel. *Biochemistry 29*, 8598–8607.
38. Casino, P., Niks, D., Ngo, H., Pan, P., Brzovic, P., Blumenstein, L., Barends, T. R., Schlichting, I., and Dunn, M. F. (2007) Allosteric regulation of tryptophan synthase channeling: the internal aldimine probed by trans-3-indole-3′-acrylate binding. *Biochemistry 46*, 7728–7739.
39. Ngo, H., Kimmich, N., Harris, R., Niks, D., Blumenstein, L., Kulik, V., Barends, T. R., Schlichting, I., and Dunn, M. F. (2007) Allosteric regulation of substrate channeling in tryptophan synthase: modulation of the L-serine reaction in stage I of the beta-reaction by alpha-site ligands. *Biochemistry 46*, 7740–7753.

40. Hawkins, A. R., and Lamb, H. K. (1995) The molecular biology of multidomain proteins. Selected examples. *Eur. J. Biochem. 232*, 7–18.
41. Bacher, I., Zidar, A., Kratzel, M., and Hohenegger, M. (2004) Channelling of substrate promiscuity of the skeletal-muscle ADP-ribosyl cyclase isoform. *Biochem. J. 381*, 147–154.
42. Lee, S. J., Ko, J. H., Kang, H. Y., and Lee, Y. (2006) Coupled expression of MhpE aldolase and MhpF dehydrogenase in *Escherichia coli*. *Biochem. Biophys. Res. Commun. 346*, 1009–1015.
43. Hwang, S., Kim, S. J., Kim, C. K., Kim, Y., and Kim, Y. C. (1999) The phnIJ genes encoding acetaldehyde dehydrogenase (acylating) and 4-hydroxy-2-oxovalerate aldolase in *Pseudomonas* sp. DJ77 and their evolutionary implications. *Biochem. Biophys. Res. Commun. 256*, 469–473.
44. Powlowski, J., Sahlman, L., and Shingler, V. (1993) Purification and properties of the physically associated meta-cleavage pathway enzymes 4-hydroxy-2-ketovalerate aldolase and aldehyde dehydrogenase (acylating) from *Pseudomonas* sp. strain CF600. *J. Bacteriol. 175*, 377–385.
45. Koon, N., Squire, C. J., and Baker, E. N. (2004) Crystal structure of LeuA from *Mycobacterium tuberculosis*, a key enzyme in leucine biosynthesis. *Proc. Natl. Acad. Sci. U.S.A. 101*, 8295–8300.